analytical chemistry

pubs.acs.org/ac Article

Single-Particle Electrochemical Biosensor with DNA Walker Amplification for Ultrasensitive HIV-DNA Counting

Fanwei Luo, Fei Chen, Yi Xiong, Zhen Wu,* Xiuhua Zhang, Wei Wen,* and Shengfu Wang

Cite This: *Anal. Chem.* 2021, 93, 4506−4512 Read Online

ACCESS | Metrics & More | Article Recommendations | Supporting Information

ABSTRACT: Single-particle electrochemical collision has gained great achievements in fundamental research, but it is challenging to use in practice on account of its low collision frequency and the interference of the complex matrix in actual samples. Here, magnetic separation and DNA walker amplification were integrated to build a robust and sensitive single-particle electrochemical biosensor. Magnetic nanobeads (MBs) can specifically capture and separate targets from complex samples, which not only ensures the anti-interference capability of this method but also avoids the aggregation of platinum nanoparticles (Pt NPs) caused by numerous coexisting substances. A low amount of targets can lead to the release of more Pt NPs and the generation of more collision current transients, realizing cyclic amplification. Compared with simple hybridization, a DNA walker can improve the collision frequency by about 3-fold, greatly enhancing detection sensitivity, and a relationship between collision frequency and target concentration is used to realize quantification. The biosensor realized an ultrasensitive detection of 4.86 fM human immunodeficiency virus DNA (HIV-DNA), which is 1−4 orders of magnitude lower than that of traditional methods. The successful HIV-DNA detection in complex systems (serum and urine) demonstrated a great promising application in real samples and in the development of new single-entity biosensors.

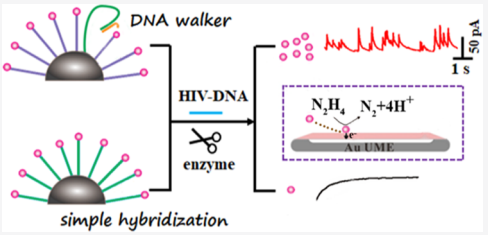

Single-particle electrochemical collision (SPEC), based on the enhancement or weakening of the current caused by the collision between single nanoparticles or biological molecules and the ultramicroelectrode (UME), has the advantages of simplicity, rapidity, wide application range, no need to separate individual particles, and continuous detection of multiple particles.[1] A UME is a class of electrodes with a one-dimensional micron or nanometer size, which was first proposed by Dayton et al.[2] Compared with conventional electrodes, the UME has many unique properties, including small size, large current density, fast mass transfer rate, fast response, low ohmic resistance drop, and high signal-to-noise ratio. In 2007, Xiao et al. first realized single Pt NP detection by the electrochemical collision between Pt NPs and a carbon fiber UME.[3] H^+ cannot be reduced on the surface of the UME at a potential of −0.5 V. However, an obvious reduction peak was collected at −0.3 V when Pt NPs collided with the UME. With the development of the UME, micromachining technology, lithography, and microscopy,[4−6] SPEC has attracted extensive attention in recent years and falls into several categories: insulating particle blockage, electrocatalytic amplification (ECA), direct oxidation of single metal or metal oxide particles, emulsion droplet reactor, vesicle reactor, intracellular vesicle impact electrochemistry, resistive pulse sensing, and so on.[7−11] In ECA, a single particle can catalyze a high concentration of a redox medium to generate obvious peak-like or step-like current to discern against the background, bringing new ideas and opportunities for developing single-particle electrochemical biosensors.

As an ultrasensitive electrochemical method, SPEC has gained great progress in the study of particle dynamics, physicochemical properties, collision mechanism, and other theoretical research,[12−15] but there are few reports for analysis application. Bard et al. used the collision between biomolecules (e.g., proteins, DNA, enzymes, or other biological macromolecules) and the Pt ultramicroelectrode to block the oxidation of $Fe(CN)_6^{4-}$ molecules on the electrode surface, which caused the reduction of current and generated current steps.[16,17] Using the linear relationship between collision frequency and target concentrations, the quantitative detection of biomolecules was realized.[4,18−20] Therefore, high collision frequency is important for the detection sensitivity of the method. But in fact, only a small number of nanoparticles in the solution can diffuse to the electrode surface to perform effective collision, suffering from the limit of low collision frequency. Thus, if target molecules are one-to-one correspondence with nanoparticle labels, collision frequency is low and it is difficult to realize sensitive detection. By combing the commonly used electrochemical signal amplification strategies (e.g., enzyme-catalyzed reaction, chain replacement, DNA

Received: November 18, 2020
Accepted: February 25, 2021
Published: March 8, 2021

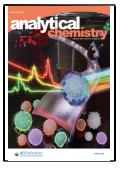

https://dx.doi.org/10.1021/acs.analchem.0c04861
Anal. Chem. 2021, 93, 4506−4512

walker, hybridization chain reaction, etc.)[21−24] with SPEC, one target binding of multiple nanoparticles (one-to-many label mode) can be achieved, which is promising to improve the detection sensitivity and solve the problem of low collision frequency in SPEC to some extent. Recently, DNA walkers have attracted wide attention because of their simple and flexible design, high efficiency, self-assembly ability, and not requiring expensive reagents. Based on SPEC, *Escherichia coli*, *Bacillus subtilis*, and viruses have also been successfully detected, which promotes the practical application of single-particle electrochemical collision.[18,25]

In clinical diagnosis, the content of the target in actual samples is low, and the interference of the complex matrix cannot be ignored. It is difficult to remove the interference of complex matrix without specific capture and separation of targets.[26] To solve this problem, Crooks et al.[27] used capture probe-modified Pt nanoparticles to achieve the specific capture of target microRNA. Then, the electrochemical collision between nanoparticles and the ultramicroelectrode was used to catalyze the oxidation of hydrazine hydrate to realize microRNA detection with a detection limit of 0.1 nM, which improved the specificity of the method to some extent. However, due to the numerous times of the washing process and the long-time centrifugation required for each process, the loss of nanoparticles is often large. Furthermore, this system can only be used for microRNA detection in buffer solution rather than serum or other complex samples, possibly because the complex matrix in samples can cause the aggregation of nanoparticles.

Aiming at the low collision frequency of SPEC and the strong interference of complex samples, a novel SPEC biosensor was developed to realize the ultrasensitive detection of HIV-DNA by combining the amplification of the DNA walker with the separation and enrichment ability of MBs. As a deadly infectious disease, sensitive and accurate detection of HIV-DNA is important for the timely diagnosis of the disease. As shown in Scheme 1, the presence of target HIV-DNA can specifically hybridize with protect DNA and pull it from the DNA walker. The opened single-stranded DNA walker immediately complemented with the support DNA on the MB surface. The addition of exonuclease III (Exo III) selectively hydrolyzed the support DNA in the double-stranded DNA, releasing Pt NPs and the single-stranded DNA walker. The single-stranded DNA walker continued to hybridrize with the support DNA, and then enzymatic digestion was triggered to perform cyclic amplification, releasing more Pt NPs into the solution. After magnetic separation, the collision experiment between the released Pt NPs and a gold ultramicroelectrode (Au UME) was performed for successful HIV-DNA detection. The DNA walker can convert trace target to numerous Pt NPs, which changed the one-to-one or many-to-one detection mode to the one-to-many amplification mode. Capture probe-modified MBs have strong magnetic response ability, stability, and dispersion in complex samples, which can achieve efficient capture and separation of targets. The introduction of MBs can improve the anti-interference ability and specificity of the system and avoid the aggregation of Pt NPs caused by the complex matrix.

EXPERIMENTAL SECTION

Seed Growing Method Synthesis of Pt NPs. Pt NPs with a diameter of 19.3 nm were prepared by the seed growing method. First, 100 mL of deionized water was boiled. Then, 7.76 mL of 0.2% $H_2PtCl_6·6H_2O$ was added and reacted for 1 min. After that, 2.37 mL of a solution containing 237 μL of sodium citrate (10%) and 237 μL of a citric acid solution (10%) was added and boiled for 30 s. Afterward, 1.18 mL of a solution containing 472 μL of the $NaBH_4$ solution (0.2%), 118 μL of sodium citrate (10%), and 118 μL of the citric acid solution (10%) was added and boiled for 10 min. Pt seeds with a diameter of 3.5 nm were obtained.

To obtain 19.3 nm of Pt NPs, 1 mL of the Pt seed solution was mixed with 29 mL of deionized water at room temperature. Then, 23 μL of a 0.4 M H_2PtCl_6 solution, 500 μL of sodium citrate (1%), and an ascorbic acid solution (1.25%) were added. The mixed solution was stirred and boiled for 30 min. After cooling to room temperature, 19.3 nm of Pt NPs were obtained.

Scheme 1. Illustration of the DNA Walker and the Magnetic Separation-Amplified Single-Particle Electrochemical Biosensor[a]

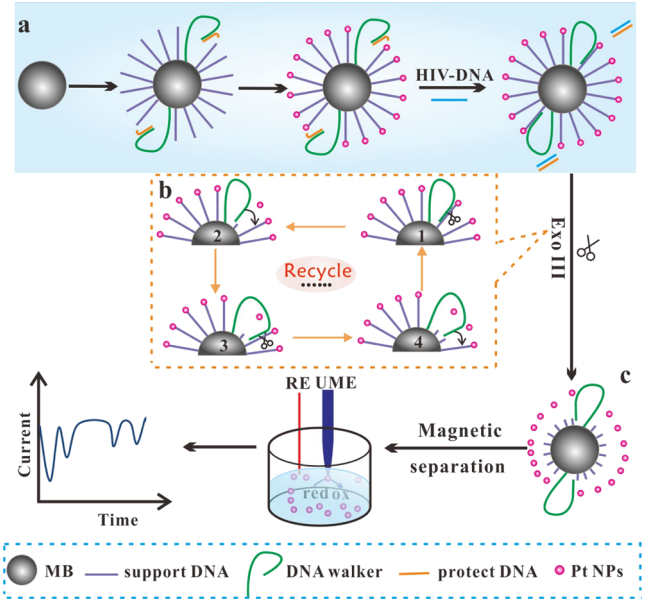

[a](a) Fabrication process of MBs−DNA−Pt NP complexes and target capture. (b) Combination of the DNA walker with Exo III for recycle amplification. (c) Released Pt NPs for current−time measurement.

Assembly of MBs−DNA−Pt NP Complexes. To obtain protect DNA−DNA walker complexes, 21 μL of the 100 μM DNA walker and 42 μL of 100 μM protect DNA were mixed and reacted for 1 h with 200 rpm at 37 °C.

Simultaneously, 40 μL of MBs was added into 200 μL of a 0.01 M phosphate buffer solution (PBS, pH = 6.1) containing 50 mM EDC and 50 mM NHS. After reacting for 0.5 h with 200 rpm at 37 °C, the solution was washed three times using a magnetic shelf. Then, 35 μL of ssDNA and 45 μL of protect DNA−DNA walker were added and reacted for 4 h to obtain MBs−DNA complexes. After being washed three times, 30 μL of 1 mM tris(2-carboxyethyl) phosphine hydrochloride (TCEP) was added and reacted for 1 h, which could remove the disulfide bond. Pt NPs were combined with ssDNA by the pH-adjusted method. Above MBs−DNA complexes were reacted with 1 mL of Pt NPs for 3 min. Then, 200 μL of a 0.1 M citrate−HCl (pH = 3) solution was added. After 5 min, 100 μL of NaCl (1 M) was added and reacted for 3 h at 4 °C. Then, MBs−DNA−Pt NP complexes were obtained, which

https://dx.doi.org/10.1021/acs.analchem.0c04861
Anal. Chem. 2021, 93, 4506−4512

were dispersed in 100 μL of 1 mM PBS (pH = 7.2) and stored at 4 °C for subsequent use.

Preparation of the Au UME. The Au UME was prepared by heat sealing a gold wire (30 μm diameter) in a glass capillary, and the preparation diagram is shown in Figure S1 in the SI. First, a gold wire with a 30 μm diameter was stuck to one end of a copper wire by silver conductive adhesive, which was inserted into a capillary with a 1 mm inner diameter. The other end of the copper wire was fixed to the capillary by glue. Second, the opening capillary tube was sealed with the help of an alcohol lamp. Then, the capillary was polished with alumina powder (0.05 μm) to obtain a disk-shaped Au UME. Last, the Au UME was sonicated three times by deionized water, alcohol, and deionized water, successively, and placed for subsequent use. The prepared Au UME was characterized by cyclic voltammetry (CV) in 5 mM $K_3Fe(CN)_6$/0.1 M KCl with a scan rate of 10 mV/s.[28]

SPEC for HIV-DNA Counting. The DNA walker, MBs, and SPEC were integrated to realize the quantitative detection of HIV-DNA. First, MBs−DNA−Pt NP complexes (20 μL), different concentrations of HIV-DNA, and 40 μL of Exo III (10 U/μL) were added into 30 μL of 1 mM PBS (pH = 7.2) and reacted for 3 h with shaking at 37 °C. After magnetic separation and washing, the supernatant containing the released Pt NPs was collected. The Pt NPs were added into 5 mL of a solution containing 10 mM N_2H_4 and 5 mM PBS (pH = 7.2) for current−time tests with a voltage of −0.1 V for 200 s. The homemade Au UME, Pt wire, and Ag/AgCl were used as the working, counter, and reference electrodes, respectively. The setting parameters of filters have an influence on the measured signals of SPEC.[29] The i/E conv filter with 32 Hz and the signal filter with 15 Hz were chosen for the collision experiments. The relationship between collision frequency (the ratio of $n_{\text{current response}}$ to time) and HIV-DNA concentrations was used for quantification.

RESULTS AND DISCUSSION

Characterization of Two Key Elements for SPEC: Pt NPs and the Au UME. SPEC is a powerful tool to characterize and detect various entities in solutions, including metal or metal oxide particles, insulating particles, biologicals, and so on. When Pt NPs stick to the UME surface, they can catalyze the inner sphere reaction[30] and produce peak-like or step-like current. Appropriate NPs and UME are critical to the successful occurrence of SPEC. Here, Pt NPs were synthesized by the seed growing method and characterized by TEM. As shown in Figure 1A,B, the Pt seeds and Pt NPs were uniform and dispersive and their average diameters were 3.5 ± 1.5 and 19.3 ± 2.4 nm, respectively, by randomly counting 200 particles. The citrate coating agent of Pt NPs with negative charges prevented nanoparticles from aggregation. Furthermore, the ultraviolet−visible (UV−vis) absorption method was applied to characterize and calculate the concentration of Pt NPs. The detailed calculation process and formula are shown in the SI, and the concentration of Pt NPs was calculated to be about 85 pM (Figure S2 in the SI), which provided an effective and accurate method to quantify the concentration of spherical Pt NPs.

In addition to Pt NPs, the preparation of the UME with an excellent electrochemical response is also important to realize SPEC. Here, the Au UME was prepared by heat sealing a gold wire (30 μm diameter) in a glass capillary. Compared with other materials, a gold wire has better ductility and chemical stability and can be easily polished, activated, and functionalized. From the CV diagram in 0.5 M H_2SO_4 (Figure 1C), there were oxidation peaks between 1.2 and 1.5 V, and a typical strong reduction peak at 0.9 V, proving the successful fabrication of the Au UME. Furthermore, the radius of the Au UME can be calculated from the limiting current of a steady-state CV obtained in 5 mM $K_3Fe(CN)_6$/0.1 M KCl with a scan rate of 10 mV/s,

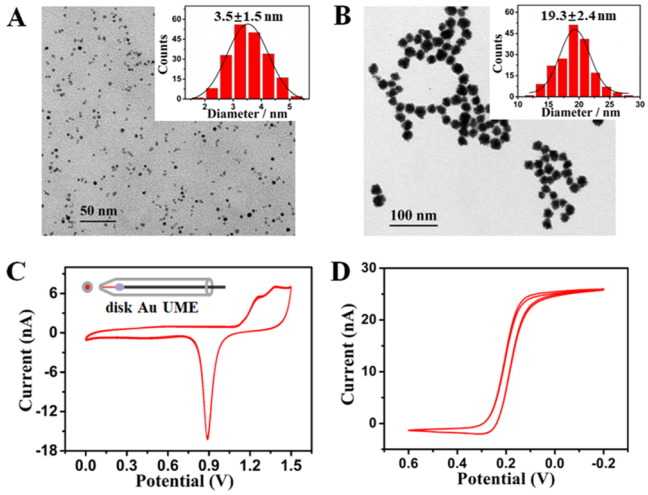

Figure 1. (A) TEM image of Pt seeds (the inset shows the size distribution). (B) TEM image of Pt NPs (the inset shows the size distribution). Cyclic voltammogram of the Au UME in 0.5 M H_2SO_4 (C) and 5 mM $K_3Fe(CN)_6$/0.1 M KCl (scan rate: 10 mV/s) (D).

$$i_{\text{lim}} = 4nFDCa \quad (1)$$

where F is Faraday's constant, D is the diffusion coefficient (7.6 × 10^{-6} cm^2/s) of ferrocyanide, and C is the concentration (5 mM) of ferrocyanide. According to a limiting current plateau of 22 nA (Figure 1D), the radius of the Au UME (a) was determined to be about 15 μm by eq 1 (the detailed calculation process is shown in Figure S4 in the SI), indicating that the Au UME was disk-shaped after being polished (Figure S3 in the SI).

In general, stable Pt NPs with a 19.3 nm diameter and a disk-shaped Au UME with a 15 μm radius were successfully prepared to perform SPEC.

Experimental and Theoretical Exploration of Single-Nanoparticle Electrochemical Collision. The electrochemical collision of single Pt nanoparticles on the Au UME surface was performed in 5 mL of a solution containing 10 mM N_2H_4 and 5 mM PBS (pH 7.2). The stability of NPs is extremely important during the collision because particle aggregation will reduce the particle concentration and the diffusion coefficient in the solution, thus reducing the collision frequency. In the experiment, PBS was added to the solution as a supporting electrolyte, which can reduce resistance drop, reduce the thickness of the diffusion layer, and act as a buffer.[30] However, the PBS concentration was found to have a great influence on particle stability, and it was optimized from 40 to 5 mM. The hydrodynamic size of Pt NPs in 40 mM PBS was up to 300 nm, which was due to the serious aggregation of NPs. In 5 mM PBS, Pt NPs had good dispersion, and the hydrodynamic size (Figure S4 in the SI) was comparable to that by TEM. Considering the buffer capacity of 5 mM PBS, the pH of the solution before and after particle collision experiments was monitored. After collision experiments, the

https://dx.doi.org/10.1021/acs.analchem.0c04861
Anal. Chem. 2021, 93, 4506−4512

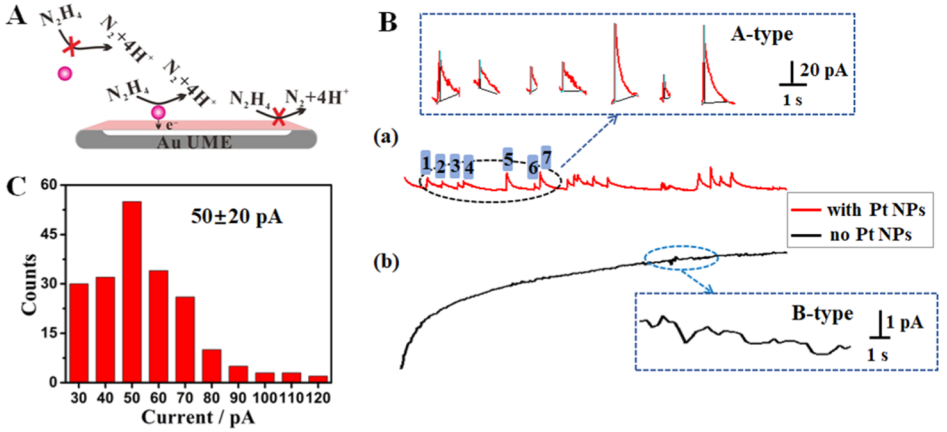

Figure 2. Single-particle electrochemical collision. (A) Electrocatalytic amplification of Pt NPs toward N_2H_4. (B) Current−time experiment with (a) and without (b) Pt NPs. (C) Current distribution (n = 200) of A-type currents.

pH of the solution changed very little, from 9.63 to 9.60. The stable pH demonstrated the sufficient buffer capacity of the PBS. Therefore, 5 mM PBS was selected. In SPEC, a suitable potential is applied to the Au UME so that N_2H_4 in the solution hardly reacts. However, when Pt NPs collide with the UME surface, it can catalyze the oxidation of N_2H_4 to produce transient currents (Figure 2A). By recording the current−time curves at different potentials, the current transients at −0.1 V were sufficiently distinct from the background noise (Figure S5A in the SI). We have tried to optimize the potential to −0.2. At −0.2 V, the background current was much smaller, but the number of current transients was much lower. Considering the importance of collision frequency to the sensitivity of the method, −0.1 V was more appropriate. It can be seen from the CV diagram of N_2H_4 on the Au UME that the limiting current of N_2H_4 was small (Figure S5B in the SI). A carbon fiber ultramicroelectrode (C UME) with a diameter of 7 μm was prepared by the same method and the experiments were repeated with the C UME (Figure S5C,D in the SI). Significantly, the homemade Au UME can be reused many times after being polished (Figure S6 in the SI), which can effectively save time and energy. Therefore, NP collision was performed by applying −0.1 V to the Au UME for 200 s.

In the absence of Pt NPs, the current−time curves were smooth and only magnified to observe rounded corners rather than peak-to-peak noise (B-type). Conversely, mainly A-type current appeared in the presence of NPs (Figure 2B), proving the feasibility of SPEC. By randomly counting 200 A-type current transients, the average value of the current was 50 ± 20 pA (Figure 2C), which was lower than the theoretical value (207 pA, the detailed calculation process was shown in Figure S7 in the SI). Possible reasons may be that the collision of Pt NPs with the Au UME is difficult from the oxidation of N_2H_4 on the Pt electrode surface, the time resolution limitation of the electrochemical workstation, and other possible factors.[20]

Feasibility and Reliability of the SPEC Biosensor. Due to the widespread application of NPs as signal labels in biosensors and its high-sensitivity-enabled single-particle counting, SPEC shows great promise in designing biosensors. The current intensity distribution of 50 ± 20 pA (Figure 2C) was a little wide and obvious fluctuation appeared. However, unlike conventional analytical methods that use signal intensities for qualification, SPEC realizes quantification based on the relationship between collision frequency (the number of current transients per unit time) and target concentration. Therefore, the influence of current fluctuation can be ignored. To explore the feasibility of SPEC in biosensor construction, collision frequencies at different NP concentrations were recorded. The collision frequency increased with Pt NP concentration (Figure S7 in the SI), indicating the probability of developing SPEC biosensors. It is worth noting that the y-intercept in Figure S7 was not 0, implying the contribution of migration. In addition to diffusion, migration may also play a role in NP movement to the UME surface. To investigate the contribution of migration, collision experiments were carried out under open-circuit conditions and potential rather than current transients were collected.[5,31] The collision frequency was about 0.59 Hz (Figure S8 in the SI), which was lower than the result based on current measurement (0.84 Hz), indicating that migration actually plays a role in the mass transfer of Pt NPs to the Au UME surface.[17]

Assume that NPs are randomly collided onto the UME surface by diffusion and the collision frequency is determined by eq 2

$$f = 4D_{NP}C_{NP}aN_A \tag{2}$$

where D_{NP} and C_{NP} are the diffusion coefficient and concentration of NPs, respectively, a is the radius of the UME, and N_A is Avogadro's number. D_{NP} can be calculated based on the Stokes−Einstein equation

$$D_{NP} = \frac{k_B T}{6\pi\eta r_{NP}} \tag{3}$$

where K_B is Boltzmann's constant, T is temperature, η is the viscosity of the solvent, and r_{NP} is the radius of the NP. Based on eqs 2 and3, the collision frequency can be calculated to be 13.5 Hz. Regardless of the contribution of migration, the experimental frequency (1.15 Hz) was an order of magnitude lower than the calculated frequency. The reasons may be as follows: (1) The collision frequency relies not only on the bulk nanoparticle concentration but also on the nanoparticle mass transport kinetics, which are mainly limited by diffusion.[32] Due to the randomness of Brownian motion, only part of nanoparticles in the solution can move to the UME surface and carry out effective collision. (2) It is difficult to count all current transients that are equal to or less than the noise level.[31]

For analytical detection, there is much interference in real samples, which not only causes the aggregation of NPs but is

https://dx.doi.org/10.1021/acs.analchem.0c04861
Anal. Chem. 2021, 93, 4506−4512

also prone to generate false results. As an effective separation material, MBs have the advantages of fast magnetic response, high capture efficiency, time saving, and no sample pretreatment. It can be seen from the TEM diagram that the particle size of MBs was relatively uniform with a regular morphology (Figure 3A). The mean size of MBs was about 457.6 nm (the inset of Figure 3A). The hysteresis loop indicated the superparamagnetism of MBs (Figure 3B). Thus, the MBs can be completely gathered on the magnetic shelf and quickly dispersed in solution without the magnetic shelf. Moreover, the magnetic capture efficiency of MBs reached 99% in 120 s (Figure 3C), demonstrating the ability of fast magnetic response, simplifying operation, and saving time. Considering the larger specific surface area and abundant functional groups on the MB surface, MBs−DNA−Pt NP conjugates were prepared. The hydrodynamic size of MBs changed from 531.2 to 615.7 nm, and the surface potential changed from −39.6 to −33.5 mV (Figure S9). Unlike the smooth surface of MBs, visible nanoparticles can be seen on the TEM image of MBs−DNA−Pt NP conjugates (Figure 3D). All data indicated the successful fabrication of magnetic complexes.

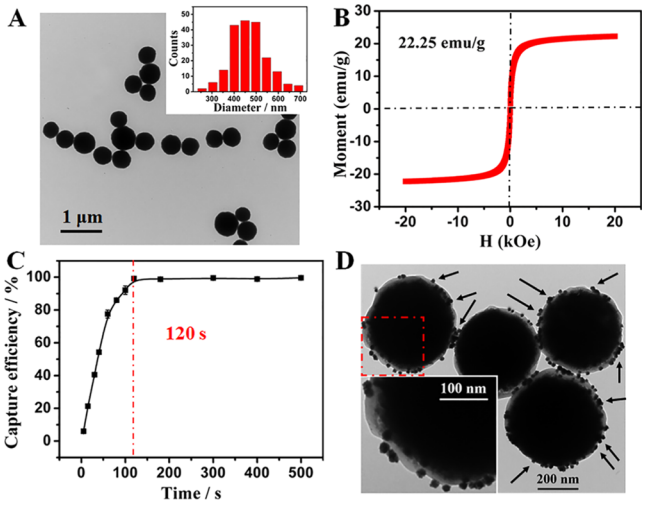

Figure 3. (A) TEM image of MBs (the inset shows the size distribution). (B) Hysteresis loop of MBs. (C) Capture efficiency of MBs on a magnetic shelf. (D) TEM image of MBs−DNA−Pt NP conjugates.

To explore the feasibility of the SPEC biosensor for HIV-DNA detection, four parallel tests were designed, including without Pt NPs, without HIV-DNA, without Exo III, and in the presence of all reagents. As shown in Figure S10, distinct current transients appeared only when all reagents were present, while no current events appeared in the other three control groups. The results proved the effective collision between the released Pt NPs and the Au UME and the reliability of the SPEC biosensor.

DNA Walker-Improved Collision Frequency. To solve the problem of low collision frequency, DNA walker amplification was introduced. Compared with the one-to-one or many-to-one mode, the one-to-many binding mode of the target to signal labels can effectively improve the detection sensitivity. Based on the simple complementary base-pairing reaction and enzyme digestion, a control experiment was designed to investigate the amplification efficiency of the DNA walker. In the control group, each target HIV-DNA released at most one NP after enzyme digestion (Figure S11 in the SI). On the contrary, the DNA walker-amplified SPEC biosensor can release 600 Pt NPs by one target (Figure S12 in the SI). When the HIV-DNA concentration was 5 nM, the number of current transients with the DNA walker was clearly more than the control group (Figure 4A). The number of current transients in current−time curves within 200 s of the two groups was calculated, and the collision frequency with (CF_1) and without (CF_2) the DNA walker was obtained by dividing the number by time. As shown in Figure 4B, CF_1 (0.74 Hz) was about 3 times as much as CF_2 (0.28 Hz). To further characterize this phenomenon, CF_1 and CF_2 of three parallel tests under different target concentrations were recorded. The result in Figure 4C showed that the DNA walker could improve the experimental collision frequency by about 3-fold.

Analytical Performance of SPEC for HIV-DNA Counting. Based on the separation ability of MBs and the capability of the DNA walker of improving the collision frequency, a novel SPEC biosensor was developed for HIV-DNA counting. As shown in Figure 5A,B, collision frequencies increased with HIV-DNA concentrations and a good linear relationship is seen between collision frequencies and the logarithm of HIV-DNA concentrations from 5 fM to 50 nM (the possible reasons for the logarithmic relationship are explained in Figure S13 in the SI). The detection limit was as low as 4.86 fM, which was 1−4 orders of magnitude more sensitive than other traditional methods for the detection of HIV-DNA, even comparable to the frequently-used method for HIV-DNA detection (Table S2 in the SI).[33−37] The excellent sensitivity and wide detection range were attributed to the following: (1) the use of MBs as capture carriers can effectively capture targets from complex samples and prevent the NPs from aggregation; (2) the combination of the DNA walker and Exo III realized a 0.843-fold enhancement of collision frequency, greatly improving the detection sensitivity; and (3) collision frequency rather than current intensity was used for

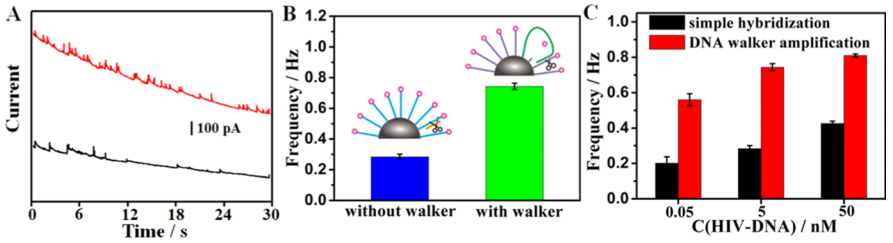

Figure 4. (A) Current−time curves of simple base-pairing hybridization (the black curve) and DNA walker amplification (the red curve) with 5 nM HIV-DNA. (B) Corresponding histogram of collision frequency. (C) Collision frequencies with (red) or without (black) the DNA walker at 0.05, 5, and 50 nM HIV-DNA.

https://dx.doi.org/10.1021/acs.analchem.0c04861
Anal. Chem. 2021, 93, 4506−4512

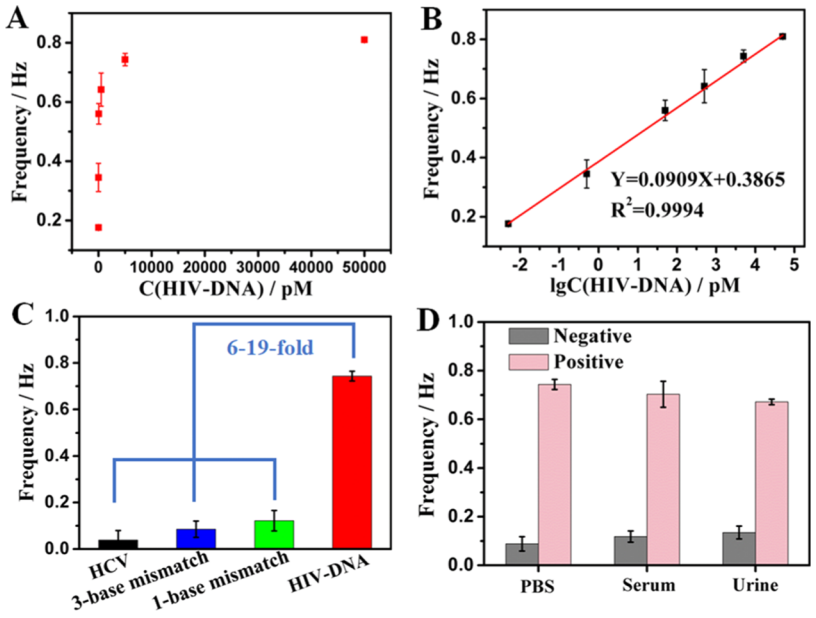

Figure 5. (A) Relationship between collision frequencies and HIV-DNA concentrations (from 5 fM to 50 nM). (B) Linear curve between collision frequencies and the logarithm of HIV-DNA concentrations. (C) Selectivity of the SPEC biosensor. (D) Collision frequencies responses for HIV-DNA in complex systems.

quantitative detection, which avoided current fluctuation and provided a reliable quantitative method.

In practical application, it is necessary for the early diagnosis and treatment of disease with high specificity. The specificity of the SPEC biosensor was explored by three interferential DNAs, including 500 nM HCV, 100 nM single-base mismatched HIV-DNA, and 100 nM three-base mismatched HIV-DNA. Even the concentrations of matched groups were 20−100-fold of HIV-DNA, and the collision frequency of HIV-DNA (5 nM) was 6−19-fold bigger than matched groups (Figure 5C). The negligible collision frequency of matched groups and even the single-base mismatched DNA can be distinguished from the target, indicating the high specificity of the SPEC biosensor.

Application of SPEC to Complex Samples. To verify the practicability of the proposed method in actual samples, the SPEC biosensor was also used for the quantification of HIV-DNA in different complex systems. The complex systems (urine or serum) contained 5 nM HIV-DNA. After magnetic separation, DNA walker amplification, and Exo III digestion, the collision frequency between the released Pt NPs and the Au UME was obtained for detection. Control groups were prepared similarly without addition of HIV-DNA. As shown in Figure 5D, the collision frequency of complex samples was comparable with PBS buffer, while the collision frequency of control groups was negligible. The result confirmed the excellent anti-interference ability of this method, resulting from the good stability and magnetic response of MBs in both buffer and the complex matrix.

CONCLUSIONS

In summary, a novel single-particle electrochemical biosensor was proposed to solve the low collision frequency of SPEC based on the DNA walker and magnetic separation, which realized HIV-DNA detection in biological systems. Collision frequency rather than current intensity was used for quantification, solving the current fluctuation of SPEC and the activity or size heterogeneity of single Pt NPs. DNA walker-assisted target recycling can enhance collision frequency by about 3-fold and 600 Pt NPs can be released by only one HIV-DNA. Moreover, the integration of magnetic separation not only ensured the capture efficiency and anti-interference capacity of the biosensor but also prevented the aggregation of Pt NPs caused by the complex system. Due to the above properties, the detection limit of the SPEC biosensor can reach femtomolar with good specificity and accuracy, which brings new chances for developing innovative SPEC biosensors and facilitating the practicability in early diagnosis and treatment.

ASSOCIATED CONTENT

Supporting Information

The Supporting Information is available free of charge at https://pubs.acs.org/doi/10.1021/acs.analchem.0c04861.

Reagents and instruments (Table S1); preparation diagram of Au UME (Figure S1); calculation of Pt NP concentration (Figure S2); CVs of different Au UMEs before and after being polished (Figure S3); hydrodynamic diameter of Pt NPs (Figure S4); optimization of detection conditions (Figure S5); reusability of Au UME (Figure S6); relationship between collision frequency and Pt NP concentrations (Figure S7); open-circuit potential (OCP) collisions of Pt NPs (Figure S8); characterization of MBs−DNA−Pt NP complexes (Figure S9); specificity of the SPEC biosensor (Figure S10); comparison between the simple base-pairing reaction and DNA walker amplification (Figures S11 and S12); and analytical performance of SPEC for HIV-DNA counting (Figure S13 and Table S2) (PDF)

AUTHOR INFORMATION

Corresponding Authors

Zhen Wu − *Hubei Collaborative Innovation Center for Advanced Organic Chemical Materials, Ministry of Education Key Laboratory for the Synthesis and Application*

https://dx.doi.org/10.1021/acs.analchem.0c04861
Anal. Chem. 2021, 93, 4506−4512

of Organic Functional Molecules, College of Chemistry and Chemical Engineering, Hubei University, Wuhan 430062, P. R. China; Email: wuzhen@hubu.edu.cn

Wei Wen − *Hubei Collaborative Innovation Center for Advanced Organic Chemical Materials, Ministry of Education Key Laboratory for the Synthesis and Application of Organic Functional Molecules, College of Chemistry and Chemical Engineering, Hubei University, Wuhan 430062, P. R. China*; orcid.org/0000-0001-6138-7470; Email: wenwei@hubu.edu.cn

Authors

Fanwei Luo − *Hubei Collaborative Innovation Center for Advanced Organic Chemical Materials, Ministry of Education Key Laboratory for the Synthesis and Application of Organic Functional Molecules, College of Chemistry and Chemical Engineering, Hubei University, Wuhan 430062, P. R. China*

Fei Chen − *Hubei Collaborative Innovation Center for Advanced Organic Chemical Materials, Ministry of Education Key Laboratory for the Synthesis and Application of Organic Functional Molecules, College of Chemistry and Chemical Engineering, Hubei University, Wuhan 430062, P. R. China*

Yi Xiong − *Hubei Collaborative Innovation Center for Advanced Organic Chemical Materials, Ministry of Education Key Laboratory for the Synthesis and Application of Organic Functional Molecules, College of Chemistry and Chemical Engineering, Hubei University, Wuhan 430062, P. R. China*

Xiuhua Zhang − *Hubei Collaborative Innovation Center for Advanced Organic Chemical Materials, Ministry of Education Key Laboratory for the Synthesis and Application of Organic Functional Molecules, College of Chemistry and Chemical Engineering, Hubei University, Wuhan 430062, P. R. China*; orcid.org/0000-0003-3586-9921

Shengfu Wang − *Hubei Collaborative Innovation Center for Advanced Organic Chemical Materials, Ministry of Education Key Laboratory for the Synthesis and Application of Organic Functional Molecules, College of Chemistry and Chemical Engineering, Hubei University, Wuhan 430062, P. R. China*; orcid.org/0000-0001-7175-4908

Complete contact information is available at: https://pubs.acs.org/10.1021/acs.analchem.0c04861

Notes

The authors declare no competing financial interest.

■ ACKNOWLEDGMENTS

This work was supported by the National Natural Science Foundation of China (Nos. 21904032 and 22076041).

■ REFERENCES

(1) Ying, Y.-L.; Ding, Z. F.; Zhan, D. P.; Long, Y. T. *Chem. Sci.* **2017**, *8*, 3338−3348.
(2) Dayton, M. A.; Brown, J. C.; Stutts, K. J.; Wightman, R. M. *Anal. Chem.* **1980**, *52*, 946−950.
(3) Xiao, X.; Bard, A. J. *J. Am. Chem. Soc.* **2007**, *129*, 9610−9612.
(4) Bai, Y.-Y.; Wu, Z.; Xu, C. M.; Zhang, L.; Feng, J.; Pang, D. W.; Zhang, Z. L. *Anal. Chem.* **2020**, *92*, 853−858.
(5) Ortiz-Ledón, C. A.; Zoski, C. G. *Anal. Chem.* **2017**, *89*, 6424−6431.
(6) Xiang, Z.; Deng, H.; Peljo, P.; Fu, Z.; Wang, S.; Mandler, D.; Sun, G.; Liang, Z. *Angew. Chem., Int. Ed.* **2018**, *57*, 3464−3468.
(7) Peng, Y.-Y.; Qian, R. C.; Hafez, M. E.; Long, Y. T. *ChemElectroChem* **2017**, *4*, 977−985.
(8) Zhang, J.-H.; Zhou, Y. G. *TrAC, Trends Anal. Chem.* **2020**, *123*, 115768−115782.
(9) Zhou, Y.-G.; Rees, N. V.; Compton, R. G. *Angew. Chem., Int. Ed.* **2011**, *50*, 4219−4221.
(10) Li, X.; Majdi, S.; Dunevall, J.; Fathali, H.; Ewing, A. G. *Angew. Chem., Int. Ed.* **2015**, *54*, 11978−11982.
(11) Pan, R.; Hu, K.; Jia, R.; Rotenberg, S. A.; Jiang, D.; Mirkin, M. V. *J. Am. Chem. Soc.* **2020**, *142*, 5778−5784.
(12) Anderson, T. J.; Zhang, B. *Acc. Chem. Res.* **2016**, *49*, 2625−2631.
(13) Oja, S. M.; Robinson, D. A.; Vitti, N. J.; Edwards, M. A.; Liu, Y.; White, H. S.; Zhang, B. *J. Am. Chem. Soc.* **2017**, *139*, 708−718.
(14) Ma, W.; Ma, H.; Chen, J. F.; Peng, Y. Y.; Yang, Z. Y.; Wang, H. F.; Ying, Y. L.; Tian, H.; Long, Y. T. *Chem. Sci.* **2017**, *8*, 1854−1861.
(15) Hafez, M. E.; Ma, H.; Ma, W.; Long, Y. T. *Angew. Chem., Int. Ed.* **2019**, *58*, 6327−6332.
(16) Dick, J. E.; Renault, C.; Bard, A. J. *J. Am. Chem. Soc.* **2015**, *137*, 8376−8379.
(17) Dick, J. E.; Hilterbrand, A. T.; Strawsine, L. M.; Upton, J. W.; Bard, A. J. *Proc. Natl. Acad. Sci. U.S.A.* **2016**, *113*, 6403−6408.
(18) Sepunaru, L.; Plowman, B. J.; Sokolov, S. V.; Young, N. P.; Compton, R. G. *Chem. Sci.* **2016**, *7*, 3892−3899.
(19) Sepunaru, L.; Sokolov, S. V.; Holter, J.; Young, N. P.; Compton, R. G. *Angew. Chem., Int. Ed.* **2016**, *55*, 9768−9771.
(20) Zhang, Y.; Mao, J.; Ji, W.; Feng, T.; Fu, Z.; Zhang, M.; Mao, L. *Anal. Chem.* **2019**, *91*, 5654−5659.
(21) Wu, Z.; Guo, W. J.; Bai, Y. Y.; Zhang, L.; Hu, J.; Pang, D. W.; Zhang, Z. L. *Anal. Chem.* **2018**, *90*, 1683−1690.
(22) Wu, Z.; Luo, F. W.; Wen, W.; Zhang, X. H.; Wang, S. F.; Wu, Z.; Luo, F. W.; Wen, W.; Zhang, X. H.; Wang, S. F. *Anal. Chem.* **2019**, *91*, 12238−12245.
(23) Guo, W.-J.; Wu, Z.; Yang, X. Y.; Pang, D. W.; Zhang, Z. L. *Biosens. Bioelectron.* **2019**, *131*, 267−273.
(24) Gao, H.; Zhang, J.; Liu, Y.; Tu, W.; Wei, T.; Dai, Z. *Anal. Chem.* **2019**, *91*, 12038−12045.
(25) Ronspees, A. T.; Thorgaard, S. N. *Electrochim. Acta* **2018**, *278*, 412−420.
(26) Labib, M.; Sargent, E. H.; Kelley, S. O. *Chem. Rev.* **2016**, *116*, 9001−9090.
(27) Castañeda, A. D.; Brenes, N. J.; Kondajji, A. K.; Crooks, R. M. *J. Am. Chem. Soc.* **2017**, *139*, 7657−7664.
(28) Wehmeyer, K. R.; Wightman, R. M. *Anal. Chem.* **1985**, *57*, 1989−1993.
(29) Kanokkanchana, K.; Saw, E. N.; Tschulik, K. *Chem. Electro. Chem.* **2018**, *5*, 3000−3005.
(30) Bard, A. J.; Faulker, L. R. In Electrochemical Methods: Fundamentals and Applications. *Russian Journal of Electrochemistry*, 2nd ed.; Wiley: New York, 2002; Vol. *38*, pp 1364−1365.
(31) Zhou, H.; Park, J. H.; Fan, F. R. F.; Bard, A. J. *J. Am. Chem. Soc.* **2012**, *134*, 13212−13215.
(32) Robinson, D. A.; Yoo, J. J.; Castañeda, A. D.; Gu, B.; Dasari, R.; Crooks, R. M.; Stevenson, K. J. *ACS Nano* **2015**, *9*, 7583−7595.
(33) Wang, L.; Tian, J.; Yang, W.; Zhao, Y.; Zhao, S. *Luminescence* **2016**, *31*, 573−579.
(34) Yan, X.; Tang, M.; Yang, J.; Diao, W.; Ma, H.; Cheng, W.; Que, H.; Wang, T.; Yan, Y. *RSC Adv.* **2018**, *8*, 31710−31716.
(35) Long, Y.; Zhou, C.; Wang, C.; Cai, H.; Yin, C.; Yang, Q.; Xiao, D. *Sci. Rep.* **2016**, *6*, No. 23949.
(36) Gao, X.; Wang, X.; Li, Y.; He, J.; Yu, H. Z. *Anal. Chem.* **2018**, *90*, 8147−8153.
(37) Deng, X.; Wang, C.; Gao, Y.; Li, J.; Wen, W.; Zhang, X.; Wang, S. *Biosens. Bioelectron.* **2018**, *105*, 211−217.